International Journal of Modern Physics B
Vol. 29, No. 13 (2015) 1550080 (10 pages)

DOI: 10.1142/S0217979215500800

Blue and green upconversion emissions of $Zr:Nd:LiNbO_3$ single crystals

Z. H. Tang*, S. P. Lin†, D. C. Ma†,§ and B. Wang*,‡

*School of Physics and Engineering, Sun Yat-sen University, Guangzhou 510275, Guangdong, P. R. China

†Sino-French Institute of Nuclear Engineering and Technology, Sun Yat-sen University, Guangzhou 510275, Guangdong, P. R. China

‡State Key Laboratory of Optoelectronic Materials and Technologies, Sun Yat-sen University, Guangzhou 510275, Guangdong, P. R. China

§madecai@mail.sysu.edu.cn

‡wangbiao@mail.sysu.edu.cn

Received 26 September 2014
Revised 14 January 2015
Accepted 27 January 2015
Published 30 March 2015

$Zr:Nd:LiNbO_3$ crystals codoped with 0.1 mol% of Nd_2O_3 and three concentrations of ZrO_2 (0, 2 and 4 mol%) were grown by the Czochralski method from the congruent melt. The X-ray diffraction (XRD) patterns, UV–visible absorption and infrared (IR) spectra were measured to analyze the crystal composition and defect structure. The blue and green upconversion emissions of Nd^{3+} ions under 598 nm excitation were observed. The intensity of upconversion emissions was increased by the introduction of 2 mol% zirconium ion (Zr^{4+}) and decreased by the introduction of 4 mol% Zr^{4+} ions. The luminescence decay measurement indicated that the $^4G_{7/2}$ state of Nd^{3+} ion was mainly populated by excited state absorption process. It was proposed that $Nd:LiNbO_3$ crystals doped with approximately 2 mol% Zr^{4+} ions could be applied as laser materials at 522/535 nm.

Keywords: $Zr:Nd:LiNbO_3$; defect structure; upconversion; rare earths.

PACS numbers: 42.25.Fx, 42.70.Mp, 61.72.Bb

1. Introduction

Nd-doped lithium niobate ($LiNbO_3$) crystal is one of the most promising laser materials that combines the extraordinary laser properties of the Nd^{3+} ion with the excellent electrooptical and nonlinear optical properties of $LiNbO_3$.[1–7] $Nd:LiNbO_3$ has gained great importance as a technological material for all-solid compact laser

§Corresponding author.

devices, solid-state tunable and self-frequency-doubled lasers.[6,7] However, little attention has been paid to the study on the upconversion emission of $Nd:LiNbO_3$ crystals for a long time. In fact, Nd^{3+} ion with 17 spectroscopic terms and 41 energy levels has a potential to provide multiple channels for upconversion process.[8,9] The development of $Nd:LiNbO_3$ as upconversion materials are of great significance for solid-state multicolor display, high-density memories, photonic applications, etc.[10–14]

In order to reduce the photorefractive effect, zirconium ion (Zr^{4+}) is added due to its low threshold (only 2 mol%) and high distribution coefficient (near one).[15,16] So Zr-doped $Nd:LiNbO_3$ makes it easy to grow crystals of good optical quality and is an excellent choice for nonlinear optical applications. Moreover, the ZrO_2 additional codoping may also influence other properties.[17,18] In particular, the Nd^{3+} ion distribution into different centers is affected by MgO or ZnO codoping, which means the luminescent center of the Nd^{3+} ion is changed.[19–23] In the case of ZrO_2 and Nd_2O_3 codoping, it is imperative to know the influence of the Zr dopant on the upconversion characteristics of the Nd^{3+} ion. This will help to improve the design and performance of Nd-doped upconversion materials based on the host $LiNbO_3$ crystal.

In the present work, $LiNbO_3$ crystals codoped with fixed Nd^{3+} ion concentrations and different Zr^{4+} ion concentrations were grown to investigate the effect of Zr^{4+} dopant on the blue and green upconversion emissions of Nd^{3+} ions under 598 nm excitation. The results show that the enhanced upconversion emission can be obtained within a certain range of the ZrO_2 dopant in $Nd:LiNbO_3$. The new type of $LiNbO_3$ crystal for frequency upconversion will extend the capacity of laser materials in the nonlinear optics field.

2. Experimental

The congruent ($Li/Nb = 48.6/51.4$) $LiNbO_3$ crystals with 0.1 mol% of Nd_2O_3 and various levels of ZrO_2 (0, 2 and 4 mol%) were successfully grown by the Czochraski technique in air along the ferroelectric *c*-axis. For convenience, the three crystals are named as ZN0, ZN2 and ZN4, respectively. The raw materials used for crystal growth were Li_2CO_3, Nb_2O_5, ZrO_2 and Nd_2O_3 whose purities were all 4N. Mixtures of the raw materials were heated at 650°C for 2 h to remove CO_2 and then further heated up to 1150°C for 2 h to form polycrystalline powder. During the growth procedure, the following optimum technology conditions were selected: the axial temperature gradient was 30–40°C/cm, the crystals were pulled along [001] direction, the pulling and rotation rates were 1–1.5 mm/h and 15 r/min, respectively. After growth, the crystals were cooled down to room temperature at a speed of 60°C/h. All the crystals exhibited smooth surface without macroscopic defects. One of the crystals was shown in Fig. 1. Finally, the crystals were cut into 10 mm × 10 mm × 3 mm (X × Y × Z) samples and polished to optical grade smoothness.

Fig. 1. (Color online) The as-grown Zr : Nd : $LiNbO_3$ crystal (No. ZN2).

The powder X-ray diffraction (XRD) patterns were analyzed by a D/MAX-2200 diffractometer with copper target ($\lambda = 0.15406$ nm) at 40 kV and 28 mA and machine scanned in the range from 20°–70°. The infrared (IR) transmittance spectra of the Zr : Nd : $LiNbO_3$ crystals were performed by a Nicolet/Nexus 670 Fourier Transform Infrared (FTIR) analyzer in the 3400–3600 cm^{-1} wavenumber range. The UV–visible optical absorption spectra of Zr : Nd : $LiNbO_3$ crystals were recorded by a UV-2501PC UV–visible spectrophotometer and the measurement range was from 300–900 nm. The upconversion fluorescence spectra and luminescence decays were recorded by a FLS920 combined fluorescence lifetime and steady state spectrometer under continuous wave (CW) or pulsed conditions. The upconversion fluorescence signal was obtained in the range from 380–550 nm. The luminescent lifetime measurement was detected in the range from 0–50 μs. All the measurements were performed at room temperature.

3. Results and Discussion

Figure 2 presents the XRD patterns of Zr : Nd : $LiNbO_3$ crystal samples, as well as the congruent $LiNbO_3$ (JCPDS No. 78-0251) to be compared with. All the diffraction peaks can be indexed as hexagonal $LiNbO_3$ with space group R3c indicate the as-grown crystals are in a single phase.[24,25] Using the XRD data, the lattice parameters of the samples were calculated by the least square method, and the unit cell volumes were obtained by the formula $V = (a^2c) \cdot \cos 30°$ as shown in Table 1. With increasing the doping Zr^{4+} ions concentration, the unit cell volumes of crystals increase at first and then decrease. According to the Li vacancy defect model,[26] there are Li vacancy (V_{Li}^{-}) and anti-site Nb (Nb_{Li}^{4+}) in congruent $LiNbO_3$ because the number of Li^+ ions is less than that of Nb^{5+} and the redundant Nb ions will occupy Li sites to form Nb_{Li}^{4+} defect groups. In ZN0, weakly doping Nd^{3+} ions replace the anti-site Nb (Nb_{Li}^{4+}) to normal Nb site. In ZN2, all Nb_{Li}^{4+} ions are replaced by Zr^{4+} ions, and this doping level is the so-called "threshold value".[15,16]

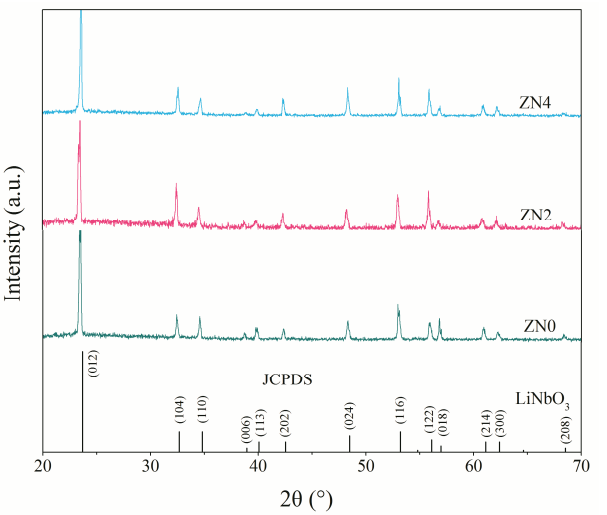

Fig. 2. (Color online) XRD patterns of $Zr:Nd:LiNbO_3$ crystals codoped with 0.2 mol% Nd^{3+} ions and various concentrations of Zr^{4+} ions (0, 2 and 4 mol%).

Table 1. Lattice constants of standard sample and $Zr:Nd:LiNbO_3$ crystals.

Samples	$a = b$/nm	σ_a^*/nm	c/nm	σ_c^*/nm	V/nm^3
CLN	0.51502	0	1.3865	0	0.31853
ZN0	0.51624	0.00026	1.3893	0.0007	0.32064
ZN2	0.51691	0.00028	1.3904	0.0006	0.32173
ZN4	0.51675	0.00017	1.3887	0.0005	0.32115

*σ is estimated standard deviation.

At the same time, all the Nd^{3+} ions occupying Nb site will be pushed to the Li site. Since the polarization abilities of Nd^{3+} and Zr^{4+} are lower than that of Nb^{5+}, the lattice constants of ZN0 and ZN2 samples increase. As for ZN4, in which the concentration of ZrO_2 is more than 2 mol%, the additional Zr^{4+} ions replace more Li^+ ions and less Nb^{5+} ions simultaneously,[27] leading to a decrease of the unit cell volume, for that the polarization abilities of Zr^{4+} are higher than that of Li^+.

The water in the raw material and air makes the H^+ ions enter the crystal to form O–H bond during the growth of crystals, which led to an IR absorption peak located at 3482 cm^{-1} in a congruent $LiNbO_3$ crystal.[28] The shifting of OH^- absorption peak reflects the location and threshold concentration of the doping ions. Figure 3 displays the IR optical transmission spectra of $Zr:Nd:LiNbO_3$ crystals with various ZrO_2 doped concentrations in the melt. The absorption peak position of ZN0 is located at 3483 cm^{-1}, while in ZN2 and ZN4 the absorption peaks are differently shifted to 3488 and 3489 cm^{-1}, respectively. In $Nd:LiNbO_3$ crystal (No. ZN0), Nd^{3+} ions substitute anti-site Nb (Nb_{Li}^{4+}) and existed in the form of Nd_{Li}^{2+}.

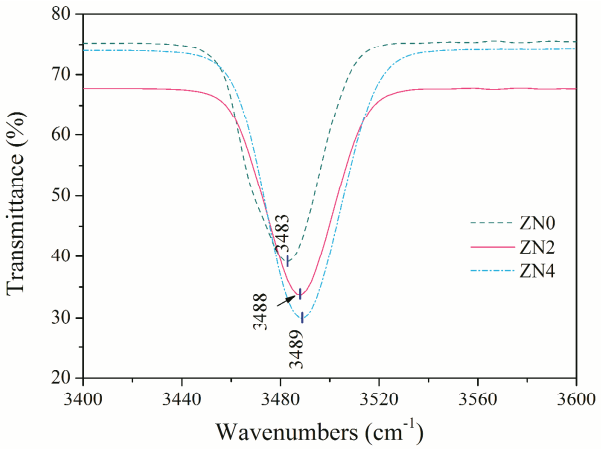

Fig. 3. (Color online) IR transmittance spectra of Zr : Nd : LiNbO$_3$ crystals codoped with 0.2 mol% Nd^{3+} ions and various concentrations of Zr^{4+} ions (0, 2 and 4 mol%).

Thus the Nd^{2+}_{Li}–OH^- defect group is formed, whose stretch vibration is corresponding to the peak slightly shifted to 3483 cm^{-1}. In the case of Zr : Nd : LiNbO$_3$ crystals (Nos. ZN2 and ZN4), it is proposed that when the concentration of ZrO_2 exceeds its threshold, all Nb^{4+}_{Li} ions have disappeared and the additional Zr^{4+} ions replace both the Li^+ and Nb^{5+} ions to form Zr^{3+}_{Li} and Zr^-_{Nb} defects for keeping the charge balance. All the Nd^{3+} ions occupying Nb site will be pushed to the Li site forming Nd^{2+}_{Li} defects. It is proposed the H^+ ions do not assemble around Zr^{3+}_{Li} and Nd^{2+}_{Li} defects because they repel each other.[29] As a result the IR absorption peaks of ZN2 and ZN4 mainly reflect the OH^- vibration in the Zr^-_{Nb}–OH^- complexes, and show obvious changes, compared with that of ZN0. Therefore, the 3488 cm^{-1} and 3489 cm^{-1} OH^- band corresponds to the Zr^-_{Nb}–OH^- complexes, since the Zr^-_{Nb} defects have a strong force to attract H^+ than V^-_{Li}.

Figure 4 shows the optical absorption spectra of various concentrations of Zr^{4+} doped Zr : Nd : LiNbO$_3$ crystal samples. It has been demonstrated that LiNbO$_3$ crystal is a kind of ferroelectrics with the oxygen octahedron structure, and the basal optical absorption edge is decided by valence electron transition energy from 2p orbits of O^{2-} to 4d orbits of Nb^{5+}. Therefore, the valence electronic state of O^{2-} has effect on the position of the absorption edge. In other words, if the polarization ability of the doping ion is lower than that of the replaced ion, which makes the polarization ability of O^{2-} decrease, the energy required by the electron transition increases and the absorption edge consequently shifts to the UV band. Otherwise, the absorption edge shifts to the IR band.[30] The partial enlarged absorption edge positions of Zr : Nd : LiNbO$_3$ crystals are illustrated in the inset of Fig. 4. The results support the idea that Li vacancy (V^-_{Li}) and anti-site Nb (Nb^{4+}_{Li}) appear because parts of Nb^{5+} occupy the Li sites in congruent LiNbO$_3$. In ZN2, the polarization ability of the doping Zr^{4+} ion is lower than that of the replaced Nb^{4+}_{Li} ion, so

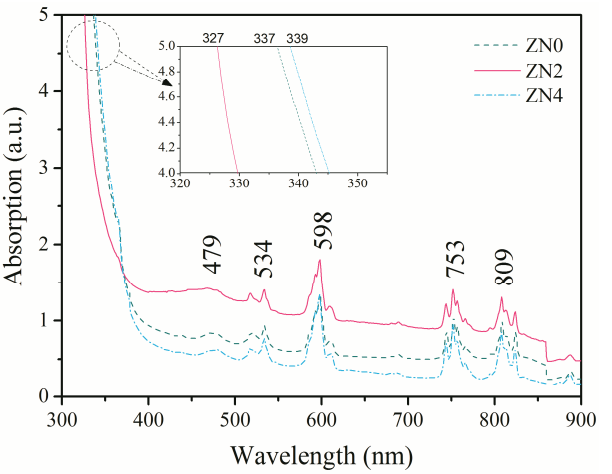

Fig. 4. (Color online) UV-visible absorption spectra of $Zr:Nd:LiNbO_3$ crystals codoped with 0.2 mol% Nd^{3+} ions and various concentrations of Zr^{4+} ions (0, 2 and 4 mol%).

Table 2. The transition spectrum of $Zr:Nd:LiNbO_3$ crystals and the corresponding energy levels.

Transition spectral	$^2G_{9/2}$	$^4G_{7/2}$	$^4G_{5/2}$	$^4F_{7/2}$	$^4F_{5/2}$
Energy levels/nm	479	534	598	753	809

the absorption edge shifts to the UV band. In ZN4, the absorption edge shifts to the IR band since the additional Zr^{4+} ions replace mostly Li^+ sites. As can be seen in Fig. 4, the absorption peak positions and shapes of three samples are nearly consistent, located at 479, 534, 598, 753 and 809 nm. The optical absorption spectra of $Zr:Nd:LiNbO_3$ crystals are composed of a variety of spectral terms, and the ground state spectral term of Nd^{3+} ion is $^4I_{9/2}$. Table 2 lists the transition spectral terms as well as the transition levels.[31] Due to the strong absorption peak of the $^4I_{9/2} \rightarrow {}^4G_{5/2}$ transition compared with that of other level transitions, a 598 nm laser is selected to measure the upconversion emission spectra.

The fluorescence spectra measured under 598 nm excitation reveals the effect of various Zr^{4+} ion concentrations on the upconversion characteristics of the Nd^{3+} ion. Figure 5(a) illustrates the measured blue and green upconversion spectra of $Zr:Nd:LiNbO_3$ crystals with the ZrO_2 concentrations of 0, 2 and 4 mol%. It is obvious that the intensities of blue and green upconversion emissions are increased at first and then decreased. In order to avoid the influence of other factors, all of the spectra were recorded under the same experimental condition, including the same pump level and the same widths of entrance. As previously discussed, weakly doping Nd^{3+} ions replace the anti-site Nb (Nb_{Li}^{4+}) to normal Nb site in ZN0. In ZN2, all Nb_{Li}^{4+} ions are replaced by Zr^{4+} ions and all the Nd^{3+} ions occupying Nb site will be pushed to the Li site. In this case, all the Nd^{3+} ions locate isolated sites, thus

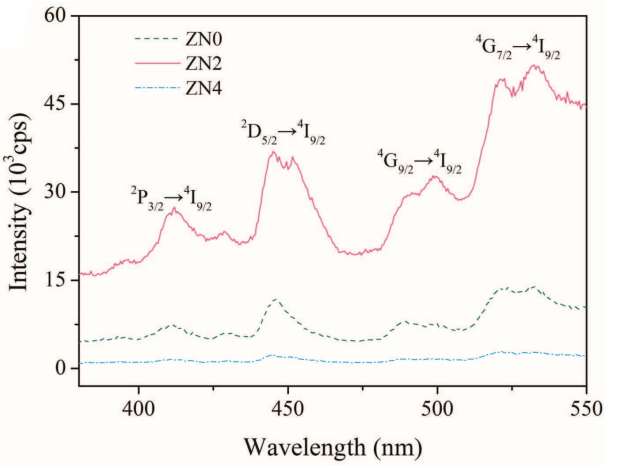

(a)

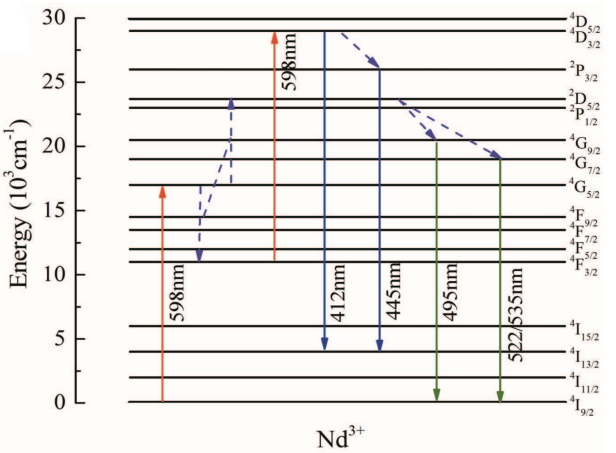

(b)

Fig. 5. (Color online) The blue and green upconversion emission spectra of Nd^{3+} ions under 598 nm excitation: (a) in ZN0, ZN2 and ZN4 crystals and (b) energy level diagram as well as the proposed upconversion process.

the luminescent center of the Nd^{3+} ion is improved and the probability of radiative transition is significantly increased. In ZN4, the high Zr^{4+} ion concentration results in the shortening of the adjacent Nd–Nd distance.[32,33] As a result, the increased cluster sites increase the probability of the nonradiative cross relaxation. Therefore, the ZN4 crystal suppresses the blue and green upconversion, while the ZN2 crystal enhances the emission, compared with the Nd : $LiNbO_3$ crystal. As can be seen in Fig. 5(a), the green emissions centered at 495 nm and 522/535 nm correspond to the $^4G_{9/2} \rightarrow {}^4I_{9/2}$ and $^4G_{7/2} \rightarrow {}^4I_{9/2}$ transitions of Nd^{3+} ion, while the blue emission centered at 412 and 445 nm are ascribed to the $^4D_{3/2} \rightarrow {}^4I_{13/2}$ and $^2P_{3/2} \rightarrow {}^4I_{13/2}$

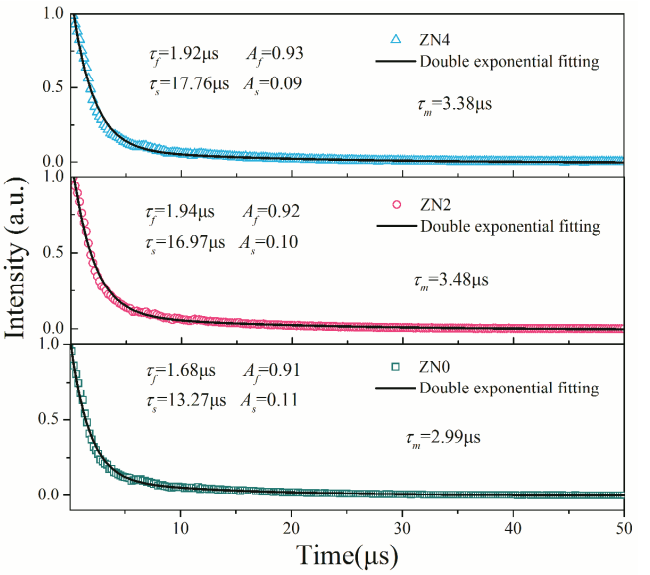

Fig. 6. (Color online) Luminescence decays of the $^4G_{7/2} \rightarrow {}^4I_{9/2}$ transition in Zr:Nd : $LiNbO_3$ crystals codoped with 0.2 mol% Nd^{3+} ions and various concentrations of Zr^{4+} ions under 598 nm excitation. The solid curves represent the best fits to experimental data using the double exponential model.

transitions, respectively. The convincing results demonstrate that approximately 2 mol% Zr^{4+} ion concentration could be good for improving the optical properties in Nd : $LiNbO_3$ crystal.

In order to understand the upconversion luminescence process for the blue and green emissions in Zr : Nd : $LiNbO_3$ crystals under 598 nm excitation, the energy level diagram of Nd^{3+} ions as well as the proposed upconversion process is drawn in Fig. 5(b). The mechanism of upconversion luminescence process is explained as follows: first, the Nd^{3+} ions in the ground state are excited to the $^4G_{5/2}$ state. Due to the long lifetime of $^4G_{5/2}$ state, a possible cross relaxation, $^4G_{5/2}+{}^4G_{5/2} \rightarrow {}^2D_{5/2}+{}^4F_{3/2}$, may occur.[34] In the second-step excitation, the Nd^{3+} ions are pumped by a second 598 nm photon from $^4F_{3/2}$ state to $^4D_{3/2}$ state. Subsequently, the $^2P_{3/2}$ state can be fed by the nonradiative relaxation of $^4D_{3/2} \rightarrow {}^2P_{3/2}$. As a consequence, the Nd^{3+} ions populating the $^4D_{3/2}$ and $^2P_{3/2}$ states relax radiatively to the $^4I_{13/2}$ level, which produce the 412 and 445 nm blue emissions, respectively. Besides, the $^4G_{7/2}$ and $^4G_{9/2}$ states can be populated by the nonradiative decay of the $^2D_{5/2}$ state, so the green emissions of Nd^{3+} ions centered at 495 and 522/535 nm are generated by radiative relaxations of $^4G_{9/2} \rightarrow {}^4I_{9/2}$ and $^4G_{7/2} \rightarrow {}^4I_{9/2}$ transitions, respectively.

Figure 6 indicates the luminescence decays of green upconversion emission at 535 nm ($^4G_{7/2} \rightarrow {}^4I_{9/2}$) of Nd^{3+} ions in the crystals with various ZrO_2 concentrations of 0, 2 and 4 mol% under 598 nm excitation. As for Zr : Nd : $LiNbO_3$ crystals,

the nonexponential behavior of the green upconversion transient is due to the cross relaxation by nonradiative energy transfer (ET).[35] Two types of fluorescing element, including the isolated Nd ions and the clustered Nd sites, contribute to the transient decay. Based on the above model, the normalized luminescence decay of the green upconversion fluorescence can be described by the double exponential function as follows:[36]

$$I(t) = I_0 + A_f e^{-t/\tau_f} + A_s e^{-t/\tau_s}. \tag{1}$$

where I_0 represents the background intensity, τ_f and A_f represent the fast components of the luminescent lifetime and the weight factor corresponding to excited state absorption (ESA), respectively, τ_s and A_s represent the slow components of the luminescent lifetime and the weight factor corresponding to ET, respectively. The ratio A_f/A_s indicates the relative contribution of ESA and ET, which are approximately equal to nine in Zr : Nd : LiNbO$_3$ crystals as can be observed in Fig. 6. Therefore, the green upconversion in Zr : Nd : LiNbO$_3$ crystals would most likely be driven by direct ESA. τ_m represents the mean decay lifetime, which could be calculated by the following function:[37]

$$\tau_m = \int_{t_0}^{\infty} \frac{I(t)}{I_{\max}} dt. \tag{2}$$

where $I_{\max}$ is the maximum of $I(t)$, which is equal to one ($t_0 = 0$). With the ZrO_2 concentration increasing, the mean decay lifetime of Zr : Nd : LiNbO$_3$ crystals are equal to 2.99, 3.48 and 3.38 μs, respectively. It is found that when the crystal with the Zr concentration is below the threshold, the luminescent lifetime would increase. Otherwise, when the crystal with the Zr concentration is above the threshold, the luminescent lifetime would decrease. It also suggests that the $^4G_{7/2}$ state of Nd^{3+} ions is mostly populated by ESA and the lifetime is related to the adjacent Nd–Nd distance. The increasing luminescent lifetime caused by 2 mol% ZrO_2 concentrations may explain the upconversion emission enhancement in ZN2.

4. Conclusion

In the present study, Zr : Nd : LiNbO$_3$ crystals with various concentrations of Zr^{4+} ions doping were grown by Czochraski technique and measured by the patterns, UV–visible absorption and IR spectra. The upconversion fluorescence spectra showed that 4 mol% Zr^{4+} ions doping Nd : LiNbO$_3$ could suppress the blue and green upconversion while the 2 mol% Zr^{4+} ions doping Nd : LiNbO$_3$ could enhance the emission. The mechanism of upconversion luminescence process of Nd^{3+} ions was discussed. The effect of the Zr dopant on the upconversion characteristics of the Nd^{3+} ion was investigated. The luminescent lifetime measurement suggested that upconversion in Zr : Nd : LiNbO$_3$ crystals would most likely be driven by ESA. It is proposed that approximately 2 mol% Zr^{4+} ions doping Nd : LiNbO$_3$ crystals could be applied as laser materials at 522/535 nm pumped under 598 nm

excitation, which is of great significance for solid-state multicolor display, high-density memories, photonic applications, etc.

Acknowledgments

The authors acknowledge the financial support of the National Natural Science Foundation of China (NSFC) (Nos. 11372361, 11302268, 10902128, 10732100, 50802026 and 10972239) and the Fundamental Research Funds for the Central Universities.

References

1. T. Y. Fan *et al.*, *J. Opt. Soc. Am. B* **3**, 140 (1986).
2. R. Wang *et al.*, *Cryst. Res. Technol.* **40**, 684 (2005).
3. R. Wang, Y. H. Xu and X. R. Liu, *Proc. SPIE* **5643**, 356 (2005).
4. R. Wang *et al.*, *Proc. SPIE* **4930**, 508 (2002).
5. J. H. Wang *et al.*, *Bull. Mater. Sci.* **32**, 183 (2009).
6. S. Kar *et al.*, *Physical B* **393**, 37 (2007).
7. M. Sekita *et al.*, *J. Appl. Phys.* **100**, 103501 (2006).
8. M. Nakamura *et al.*, *J. Cryst. Growth* **290**, 144 (2006).
9. J. Capmany *et al.*, *Opt. Commun.* **161**, 253 (1999).
10. V. Krasnoholovets, N. Kukhtarev and T. Kukhtareva, *Int. J. Mod. Phy. B* **20**, 2323 (2006).
11. K. S. J. Wilson and K. Navaneethakrishnan, *Int. J. Mod. Phy. B* **25**, 1681 (2011).
12. T. Zhang *et al.*, *Optik* **115**, 197 (2004).
13. T. Zhang *et al.*, *Mater. Chem. Phys.* **103**, 137 (2007).
14. J. E. Midwinter and J. Warner, *J. Appl. Phys.* **38**, 519 (1967).
15. Y. F. Kong *et al.*, *Appl. Phys. Lett.* **91**, 081908 (2007).
16. N. Argiolas *et al.*, *J. Appl. Phys.* **108**, 093508 (2010).
17. J. O. Tocho *et al.*, *Solid State Commun.* **80**, 575 (1991).
18. G. Lifante *et al.*, *Chem. Phys. Lett.* **176**, 482 (1991).
19. J. G. Solé *et al.*, *J. Phys. IV* **1**, C7-403 (1991).
20. E. Camarillo *et al.*, *Phys. Rev. B* **45**, 4600 (1992).
21. H. Zacharias, *Int. J. Mod. Phy. B* **04**, 45 (1990).
22. C. Prieto, *Opt. Mater.* **12**, 135 (1999).
23. H. Kimura *et al.*, *Int. J. Mod. Phy. B* **23**, 3631 (2009).
24. R. C. Miller and A. Savage, *Appl. Phys. Lett.* **9**, 169 (1966).
25. D. C. Ma *et al.*, *Mod. Phys. Lett. B* **21**, 207 (2007).
26. P. Lerner, C. Legras and J. P. Dumas, *J. Cryst. Growth* **3**, 231 (1968).
27. Z. F. Zhou *et al.*, *Opt. Laser Technol.* **44**, 337 (2012).
28. X. H. Zhen, L. C. Zhao and Y. H. Xu, *Appl. Phys. B* **76**, 655 (2003).
29. L. Dai *et al.*, *Chen, Mater. Res. Bull.* **53**, 132 (2014).
30. M. Wöhlecke, G. Corradi and K. Betzler, *Appl. Phys. B* **63**, 323 (1996).
31. G. F. Wang *et al.*, *Phys. Rev. B* **60**, 15469 (1999).
32. D. L. Zhang *et al.*, *Appl. Phys. B* **95**, 335 (2009).
33. J. J. Ju *et al.*, *J. Opt. Soc. Am. B* **20**, 1990 (2003).
34. G. F. Wang, *J. Opt. Soc. Am. B* **18**, 173 (2001).
35. P. J. Hardman *et al.*, *IEEE J. Quantum Electron.* **35**, 647 (1999).
36. J. J. Ju *et al.*, *Appl. Phys. Lett.* **69**, 1358 (1996).
37. L. Sun *et al.*, *Appl. Phys. Lett.* **91**, 071914 (2007).